

# Transport properties of bi-epitaxial $\text{YBa}_2\text{Cu}_3\text{O}_{7-\delta}$ grain boundary Josephson junctions: Experimental evidence of a subdominant superconducting phase

Simon K. H. Lam and Sabaratnasingam Gnanarajan

*CSIRO Materials Science and Engineering, P.O. Box 218, Lindfield, New South Wales 2070, Australia*

(Received 9 November 2007; revised manuscript received 4 March 2008; published 29 September 2008)

We present the fabrication of a  $45^\circ$  [001] tilted asymmetrical bi-epitaxial  $\text{YBa}_2\text{Cu}_3\text{O}_{7-\delta}$  grain boundary Josephson junction using yttria-stabilized zirconia as the seed layer. The magnetic-field dependence of the critical current,  $I_c(B)$ , of these junctions was measured over a wide range of temperatures. Significant asymmetry of the  $I_c(B)$  with respect to the magnetic-field polarity was observed at low temperatures. Our measured results are compared with theoretical predictions of Josephson-junction behavior based on  $d$ -wave superconducting electrodes with the onset of a subdominant symmetry component. We estimate an imaginary subdominant symmetry greater than 20% to the  $d$  wave.

DOI: [10.1103/PhysRevB.78.094521](https://doi.org/10.1103/PhysRevB.78.094521)

PACS number(s): 74.20.Rp, 74.50.+r

## I. INTRODUCTION

Some experiments have demonstrated that the dominant pair symmetry of the order parameter in high-temperature superconductors (HTSCs) is the  $d_{x^2-y^2}$  wave.<sup>1,2</sup> It has been suggested that mixed order-parameter symmetry (MOPS) can exist on the surface or interfaces where the dominant pair symmetry is suppressed.<sup>3,4</sup> One unique characteristic of the  $d_{x^2-y^2}$  wave is the presence of a node along the (110) direction. In the presence of an interface perpendicular to this direction, there is a  $\pi$  phase shift for the Andreev-reflected quasiparticles, which creates the zero-energy bound states (ZEBs) on the interface. These ZEBs can suppress the  $d_{x^2-y^2}$  wave, and other types of pair symmetry will be created.<sup>4,5</sup> Experimentally, the Josephson effect is an important test bed of the MOPS due to its phase-sensitive properties.<sup>1,6</sup>

The splitting of the zero-voltage bias peak in tunneling spectroscopy has indicated strong evidence of MOPS.<sup>7,8</sup> On the other hand, it had been proposed that spontaneous circulating currents will be generated on a superconducting quantum interference device (SQUID) in the presence of MOPS (Ref. 9) and was experimentally realized very recently by Kirtley *et al.*<sup>10</sup> using  $\text{YBa}_2\text{Cu}_3\text{O}_{7-\delta}$  (YBCO)/Au/Nb junctions. However, the second-order parameter was found to be less than 2.5% of the dominant  $d_{x^2-y^2}$  wave in optimally doped YBCO. Another type of experiment to investigate the possibility of MOPS through a phase-sensitive test is to study the magnetic-field dependence of the critical current,  $I_c(B)$ , of asymmetric  $45^\circ$  junctions with a randomly faceted interface along the junction. The  $I_c(B)$  patterns of this type of junction with pure  $d_{x^2-y^2}$  pair symmetry were first modeled by Copetti *et al.*<sup>11</sup> Neils and Van Harlingen<sup>12</sup> extended this model to the cases of  $d_{x^2-y^2}$  plus subdominant pair symmetry ( $s$  and  $d_{xy}$ ) and concluded that the onset of the subdominant out-of-phase pair symmetry would manifest itself as an asymmetric diffraction pattern on field polarity, which is a direct indication of MOPS. However, their experimental results on YBCO and  $\text{Bi}_2\text{Sr}_2\text{Ca}_1\text{Cu}_2\text{O}_{8+x}$  asymmetric  $45^\circ$  bicrystal grain boundary junctions did not show the expected asymmetry over a wide temperature range.<sup>12,13</sup> A similar analysis was performed on YBCO/Nb zigzag junctions by

Smilde *et al.*<sup>14</sup> and their experimental results suggested that an imaginary  $s$ -wave contribution is less than 1%. Therefore, there is still a large discrepancy on the presence of MOPS using different experimental techniques.

A big challenge for HTSC grain boundary junctions is the achievement of a uniform barrier interface with minimum faceting effect.<sup>15,16</sup> The faceting effect is believed to be controlled by the YBCO growth mechanism on the two electrodes of the junctions and the quality of the substrate grain boundary interfaces. Bicrystal junctions that have been widely used to study the transport properties of grain boundary junctions as substrates with different tilting orientations are available commercially. A recent report from Testa *et al.*<sup>17</sup> showed that a  $0-\pi$  phase change can only be observed when the junction width was reduced to less than 500 nm. The observation of an intrinsic  $\pi$  phase change is an indication of the formation of ZEBs on the junction interface, leading to an anomalous nonmonotonic temperature dependence of the critical current. The authors argued that the effects of faceting and defects at the interface in wide junctions, resulting in an inhomogeneous interface and high transparency channels, are expected to be reduced in smaller junctions. Their junctions were fabricated using  $45^\circ$  tilted symmetrical bicrystal substrates. Recent experiments on the study of cerium oxide ( $\text{CeO}_2$ ) bi-epitaxial junctions indicate that it has a tunnel-like junction behavior with a barrier of very low transparency<sup>18</sup> and could be a good candidate to study the order parameter of HTSC materials.

Yttria-stabilized zirconia (YSZ) has the same crystal structure as the  $\text{CeO}_2$  but with a slightly smaller lattice constant<sup>19</sup> and can also be used as the seed layer for the fabrication of bi-epitaxial junctions. Our group has been working on YBCO step-edge junctions and YBCO/YSZ superconducting tape in the past decade.<sup>20,21</sup> We started to investigate the fabrication of asymmetric  $45^\circ$  [001] tilted grain boundary junctions by combining our techniques on making high-quality step edges and depositing high-quality YSZ to produce a bi-epitaxial junction. In this paper, we present fabrication techniques and measurements of  $45^\circ$  grain boundary junctions on MgO substrates using different thicknesses of YSZ as the seed layer. The critical-current-magnetic-field dependence,  $I_c(B)$ , of our junctions does not show the conven-

tional Fraunhofer-type pattern. The junctions, which have a lower value of  $J_c$ , showed a change in symmetry in field polarity with decreasing temperatures, indicating the onset of a complex secondary pairing component. On the other hand, the junction with a higher value of  $J_c$  did not show this change.

## II. THEORETICAL MODELING

The  $I_c(B)$  patterns of an asymmetric  $45^\circ$  junction with pure  $d_{x^2-y^2}$  pair symmetry were first modeled by Copetti *et al.*<sup>11</sup> Due to the faceting effect, the junction consisted of multiple miniature junctions with different orientations with respect to the nodal direction of the electrode with  $45^\circ$  rotation. As there is a  $\pi$  phase change from one lobe to the adjacent lobe, some of the miniature junctions have additional  $\pi$  phase shift across the junction. The  $I_c(B)$  dependence of the whole junction can be derived from the integral of the field dependence of individual miniature junctions,<sup>11</sup>

$$I_c(B) = \int_{-w/2}^{w/2} J_c(y) \sin\left(2\pi \frac{\Phi(y, B)}{\Phi_0} + \phi(y) + \phi_0\right) dy, \quad (1)$$

$$J_c(y) = (2K/\hbar) \psi_{02}(y) \psi_{01}(y). \quad (2)$$

Here,  $w$  is the width of the junction along the  $y$  axis,  $\phi(y)$  is the additional phase shift of each miniature junction, and  $\phi_0$  is the global phase difference between the two electrodes (subscripts 01 and 02).  $J_c(y)$  is the critical-current density of the miniature junction.  $\psi$  is the amplitude of the order parameter and  $K$  is the coupling constant. In our calculation of  $I_c(B)$ , the junction is divided into certain number of facets with different facet lengths and orientations. In this analysis, the self-field generated by the junction current is not included. This is valid as long as the junction width is small compared with the Josephson penetration depth.

Figure 1(a) shows the simulation of a  $4 \mu\text{m}$  wide asymmetric  $45^\circ$  junction with pure  $d_{x^2-y^2}$  pair symmetry of 20 facets using Eqs. (1) and (2). Although the simulated pattern is unique for each particular facet pattern, the common feature is that the pattern does not have a conventional Fraunhofer pattern. Instead it has a maximum at nonzero magnetic field and is symmetrical with the field polarity,<sup>11</sup> which is consistent with the patterns observed on different types of asymmetric  $45^\circ$  junctions.<sup>12,15</sup> The introduction of a secondary order parameter (on electrode 02) with the same facet pattern only requires the recalculation of  $\phi(y)$  and  $\psi_{02}(y)$  in Eqs. (1) and (2). Figure 1(a) also shows the simulation of  $I_c(B)$  patterns of the same facet pattern with a mixed order parameter of  $0.8d+0.2is$ . The introduction of the imaginary  $s$  component induces an asymmetrical effect on the field polarity particularly at low fields.<sup>12</sup> The asymmetry is due to  $\phi(y)$ , which has a value of  $0 < \phi(y) < \pi$  (instead of zero or  $\pi$  in the case of pure  $d$  wave) as  $\psi_{02}(y)$  is now fully gapped due to the presence of the second-order parameter.

Apart from the onset of a secondary order parameter, we also investigated the temperature dependence of  $I_c(B)$  due to the temperature dependence of  $\psi$ ,  $\psi(T) = \psi_0 [1 - (T/T_c)^2]$ . Here,  $\psi_0$  is the amplitude of  $\psi$  at zero temperature and  $T_c$  is

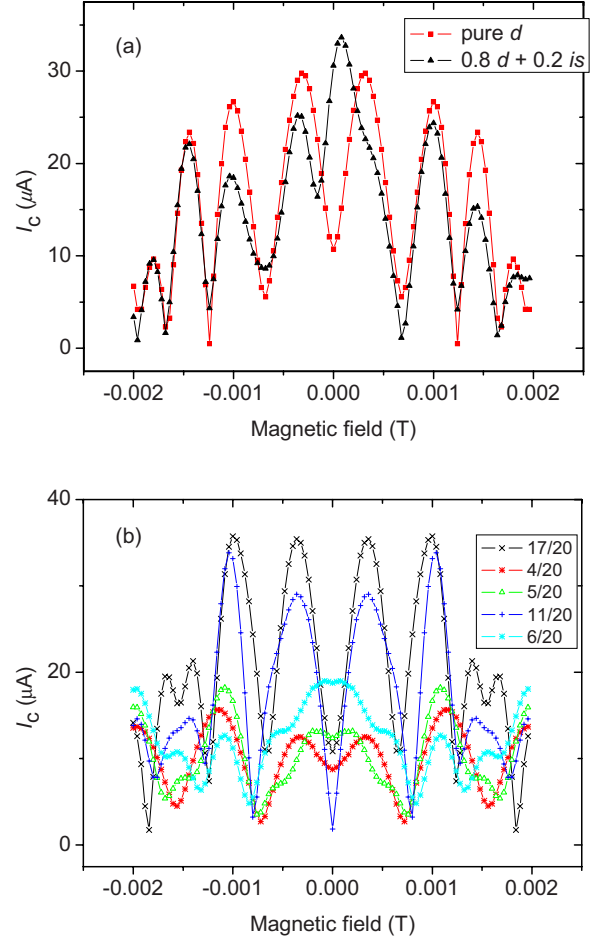


FIG. 1. (Color online) Calculated  $I_c(B)$  patterns (a) of a  $45^\circ$  asymmetrical  $4 \mu\text{m}$  wide junction with 20 facets for pure  $d_{x^2-y^2}$  wave and a mixture of  $0.8d_{x^2-y^2}+0.2is$  and (b) of another junction with 20 facets when more facets (from 4 to 17) contribute  $I_c$  to the junction.

the critical temperature.  $\psi(T)$  is calculated from BCS theory in the weak-coupling limit. The amplitude of  $I_c(B)$  increases with decreasing temperature due to  $\psi(T)$  [Eq. (2)], but the pattern itself is maintained for a particular facet structure in the case of a single value on both  $\psi_{01}(y)$  and  $\psi_{02}(y)$ . However, it has been suggested that  $\psi$  would be suppressed at the interface due to the misalignment of  $\psi_{01}(y)$  and  $\psi_{02}(y)$ . The length scale of this suppression can be as far as the scale of the coherence length from the boundary.<sup>22</sup> Structural disorder also occurs at the interface.<sup>23,24</sup> These all cause a variation in both  $\psi_0$  and  $T_c$  of each facet. On the other hand, due to the presence of microscale inhomogeneity along the grain boundary, it is expected that the facets on the junction will have a range of values for the coupling constant,  $K$ . Some of the facets with a lower value of  $K$  will not contribute significant  $J_c(y)$  through the junction at high temperature as  $\psi$  is small [Eq. (2)]. As the temperature decreases, these facets will start to contribute significant  $J_c(y)$  when  $\psi$  increases.

A quantitative analysis for the temperature dependence of  $I_c(B)$  is impossible as the detail of the local structure is unknown. We attempted to perform a qualitative analysis by introducing a factor,  $\chi$ , on the right-hand side of Eq. (2) to

account the factors of the temperature dependence of  $J_c(y)$  discussed in the previous paragraph.  $\chi$  is set to either 1 or 0.1 for each facet. We then calculated  $I_c(B)$  when some of the facets'  $\chi$  value changed from 0.1 to 1 [Fig. 1(b)]. This will qualitatively simulate the fact that some of the facets start to contribute the component of  $J_c(y)$  in the  $I_c(B)$  calculation when the temperature decreases. It was found that the field polarity symmetry was maintained in the case of pure  $d_{x^2-y^2}$  order symmetry. However, an additional modulation period within the main envelope developed. In some cases, a dip at zero field will change to a peak and then change to a dip again as more facets contribute  $I_c$  to the junction [Fig. 1(b)]. This happens because each facet has either zero or an additional  $\pi$  phase shift, which constitutes either a positive or negative  $I_c$  value.

### III. EXPERIMENT

Our bi-epitaxial substrates were made using MgO(001) substrates with a YSZ seed layer. YSZ seed layers about 100 nm thick were grown on MgO substrates at room temperature using a magnetron thin-film deposition system. The substrates were bombarded with Ar ions at an angle of  $55^\circ$  from the substrate normal during the YSZ deposition to induce epitaxial growth.<sup>21</sup> The ion-beam assisted deposition produced smooth and dense films.<sup>25</sup> The substrates were mounted with the (110) planes oriented in the ion-beam direction which resulted in an epitaxial YSZ layer with MgO(110) and YSZ(110) planes aligned.

The YSZ layers were patterned using photolithography and ion-beam etching to remove part of the YSZ layer. The substrate was then cleaned by a low energy (300 V) ion beam before being coated with a 200 nm YBCO and 50 nm gold films by Theva GmbH.<sup>26</sup> This process was also used to change the thickness of the YSZ before the YBCO deposition. The YBCO films were investigated using x-ray diffraction (XRD)  $\theta$ - $2\theta$  scan, rocking curve, and  $\varphi$ -scan measurements to study the grain orientation. The gold film over the junction area was removed by ion-beam etching. Junctions with widths either 3.5 or 8  $\mu\text{m}$  were formed by photolithographic patterning process with ion-beam etching. The substrate was cooled at liquid nitrogen temperatures using a cold stage during the YBCO ion-beam etching to minimize the degradation of the junction due to ion-beam-induced heating effects.<sup>20</sup> The junctions were then characterized by measuring their current-voltage and  $I_c(B)$  dependence at different temperatures in a liquid-helium dewar. The measurements were performed using a home-built probe with a single layer mu-metal shield. The stability of the temperature was controlled by positioning the probe at different levels above the helium liquid with temperature fluctuations of less than 50 mK. Here, we report on junctions fabricated from four different chips A, B, C, and D. Chips A, B, and D had a similar value for the YSZ thicknesses of  $\sim 100$  nm, whereas chip C had a much thinner YSZ film thickness of  $\sim 30$  nm. We noticed that the junctions fabricated from these two groups of different YSZ thicknesses have significant differences in their electrical parameters and  $I_c(B)$  patterns.

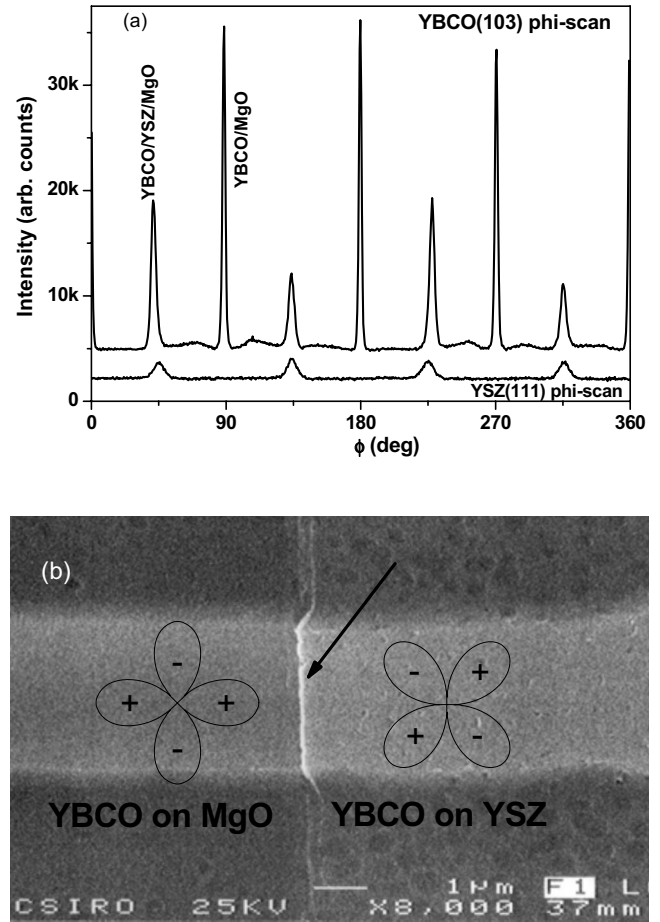


FIG. 2. (a) The YBCO(103) and YSZ(111)  $\varphi$  scans of a YBCO/YSZ/MgO sample A (Table I). (b) A scanning electron micrograph of a  $45^\circ$  asymmetrical grain boundary junction. The junction is  $\sim 3.5$   $\mu\text{m}$  wide and the arrow points to the junction interface.

## IV. RESULTS AND DISCUSSION

### A. Crystallographic structure

We have performed XRD  $\theta$ - $2\theta$  scan of all the YBCO/YSZ/MgO(001) chips. The presence of strong (003), (004), and (006) YBCO peaks indicated  $c$ -axis growth of YBCO. To determine the YBCO grain alignment on YSZ and MgO surface, the XRD measurement of YBCO(006) rocking curve was fitted with two peaks of different widths. The sharp peak with full width at half maximum (FWHM) of  $0.53^\circ$  is due to the YBCO on a bare MgO substrate and the broad peak with FWHM of  $2.0^\circ$  is due to the YBCO/YSZ/MgO. Figure 2(a) shows the YBCO(103) and YSZ(111)  $\varphi$  scans on one of the chips. The sharp peaks with FWHM of  $1.9^\circ$  are due to YBCO films on the bare MgO substrate and the broader peaks with FWHM of  $3.2^\circ$  are due to YBCO film on YSZ layer which is aligned with the YSZ(111) peaks. The above results indicated YBCO films with  $45^\circ$  difference in crystallographic orientation were successfully coated on MgO substrates using YSZ seed layers [Fig. 2(b)]. The critical-current density of the YBCO film on both MgO and YSZ seed layer was measured by an induction coil method in Theva GmbH and found to have a value greater than 1 MA/cm<sup>2</sup> at 77 K.

TABLE I. A summary of the junctions' electrical parameters. Junctions with the same prefix letter are on the same chip and  $t$  is the YSZ thickness. The  $J_c$  values were calculated from the measured  $I_c$  values when no external magnetic field was applied.

Junction	$w$ ( $\mu\text{m}$ )	$t$ (nm)	$J_c$ ( $10^3$ A/cm $^2$ )	$R_n$ ( $\Omega$ )	$R_n A$ ( $10^{-8}$ $\Omega$ cm $^2$ )	$\lambda_J$ ( $\mu\text{m}$ )
A1	8	100	2.5	3.5	4.1	6.1
A2	8	100	3.5	9.4	5.6	5.1
A3	8	100	4.9	4.2	7.8	4.3
A4	8	100	1.6	8.8	14.1	7.6
B1	3.5	100	1.2	10.7	7.5	8.8
B2	3.5	100	0.15	13.4	9.4	24.8
C1	3.5	30	5.2	1.2	0.84	4.2
D1	3.5	100	0.7	9.6	6.7	11.5
D2	3.5	100	1.4	8.9	6.2	8.1

### B. Current-voltage characteristics

Table I summarizes the electrical parameters of the junctions reported here. Figure 3 shows the current-voltage characteristics (IVCs) at 4.3 K of three junctions from the three

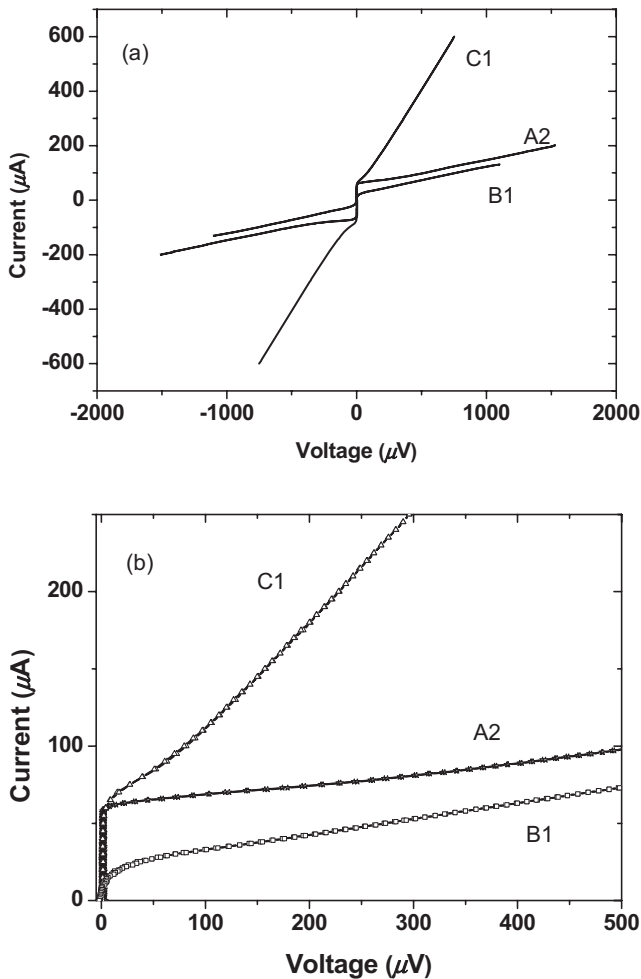


FIG. 3. (a) The current-voltage characteristics of junctions A2, B1, and C1 at 4.25 K after samples were cooled in zero field. (b) A magnified figure of (a).

different chips. All the IVCs showed typical resistively shunted junction behavior.<sup>27</sup> The critical-current density,  $J_c$ , has a range of values of  $\sim(0.2-4) \times 10^3$  A/cm $^2$ , which is in the same order of magnitude as other  $45^\circ$  [001] tilted junctions fabricated by different techniques.<sup>15,28</sup> The specific resistivity value  $R_n A$  (where  $R_n$  and  $A$  are the normal resistance and area of the junction, respectively) is of the order of  $10^{-7}$   $\Omega$  cm $^2$ , which is similar to other  $45^\circ$  [001] tilted junctions.<sup>15</sup> The spread of  $J_c$  and  $R_n$  values is believed to be due to the microscopic details of the individual junctions, including the grain orientation and faceting along the width of the junction. However, the low  $J_c$  values of the junctions indicate that the majority of tilted angles would be close to  $45^\circ$ . The Josephson penetration depth of the junction is given by  $\lambda_J = \{\Phi_0 / [2\pi\mu_0 J_c (t + 2\lambda)]\}^{1/2}$ . Here,  $\lambda$  is the bulk London penetration depth of YBCO, which is  $\sim 140$  nm.<sup>29</sup>  $\mu_0$  is the vacuum permeability and  $t$  is the junction interlayer layer thickness. The exact value of  $t$  is unknown but is believed to be  $\sim 3$  nm. The  $\lambda_J$  value of junctions A1–A4 has a range of 4.3–7.6  $\mu\text{m}$ , which is slightly smaller than the physical width of 8  $\mu\text{m}$ . Therefore, A1–A4 are not in the “short-junction” limit and the self-field effect cannot be completely excluded. The self-field effect would alter the  $I_c(B)$  patterns due to more current flowing along the junction’s edges. We also fabricated another five junctions B1, B2, C1, D1, and D2 with widths of 3.5  $\mu\text{m}$  from another three chips. The  $\lambda_J$  values of these narrower junctions are in the range of 4.2–24.8  $\mu\text{m}$ . The junctions are in the short-junction limit and the self-field effect can be excluded. The electrical parameters of the nine junctions are summarized in Table I. In addition, C1 has a  $R_n A$  value of approximately ten times smaller than the other junctions. We noticed that the change in  $I_c(B)$  pattern with temperature on C1 is quite different to the other junctions, which will be discussed.

### C. Critical current-magnetic-field characteristic

For Josephson junctions with homogeneous current flowing across the area, the  $I_c(B)$  dependence has a hallmark Fraunhofer-type behavior.<sup>27</sup> However, the  $I_c(B)$  patterns in  $45^\circ$  asymmetric junctions are different.<sup>15</sup> We have measured

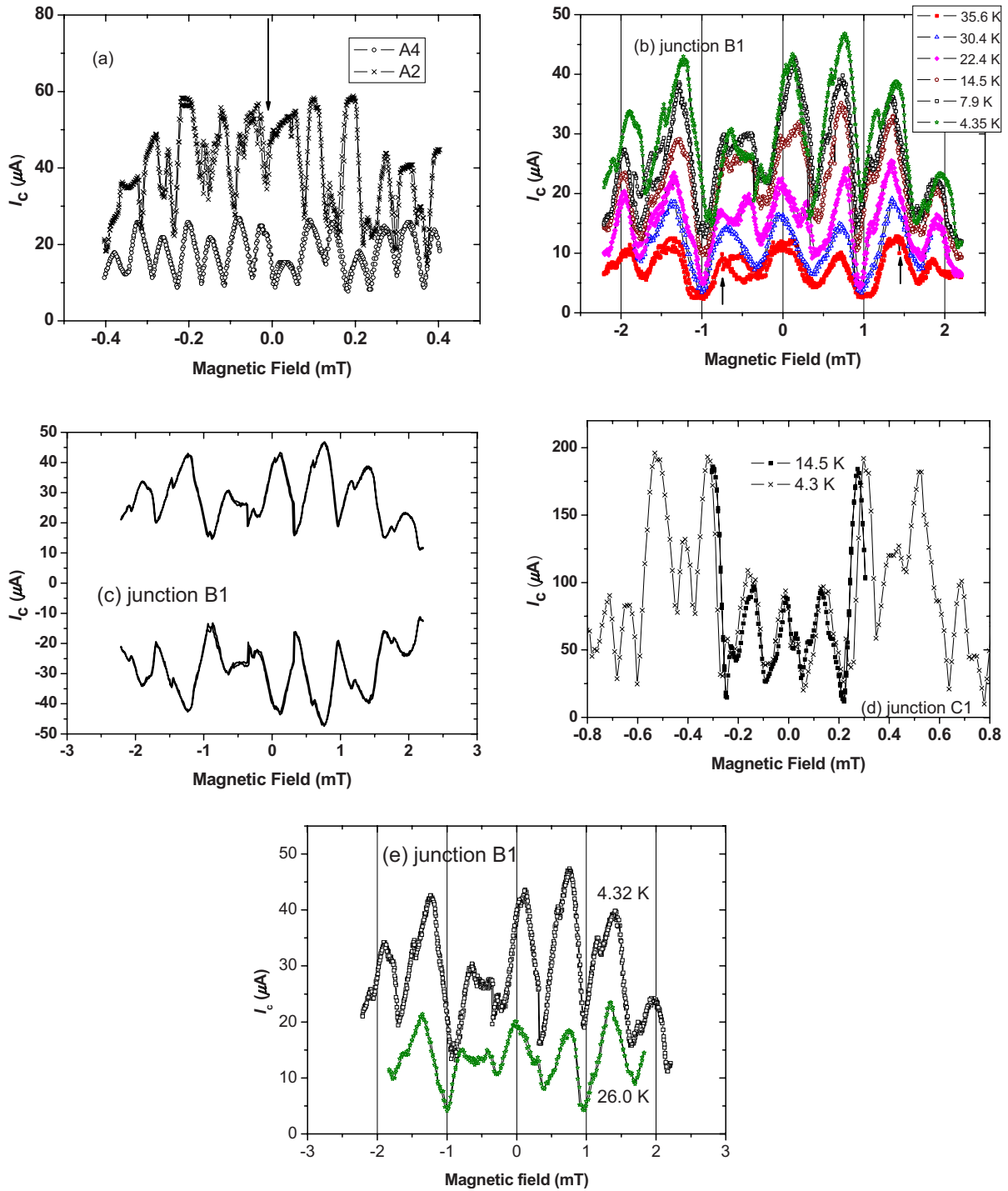


FIG. 4. (Color online) (a)  $I_c(B)$  of A2 and A4 at 4.3 K. The arrow indicates an apparent symmetrical point at  $\sim -10 \mu\text{T}$ . (b)  $I_c(B)$  of B1 at different temperatures. Arrows indicate flux jump (see text). (c) The positive and negative  $I_c(B)$  of B1 at 4.3 K. (d)  $I_c(B)$  of C1 at different temperatures. (e)  $I_c(B)$  of B1 at two different temperatures after the sample has been warmed up to  $\sim 100 \text{ K}$  (above its critical temperature) and cooled down.

the  $I_c(B)$  characteristics of all nine junctions (Table I). None of them showed typical Fraunhofer-type behavior. Figures 4(a)–4(d) show the  $I_c(B)$  patterns of junctions A2, A4, B1, and C1. The critical current was recorded using a voltage criterion of  $5 \mu\text{V}$  as the magnetic field increased to a maximum value and decreased to the minimum before increased back to zero. There are common features among our  $I_c(B)$

curves. First, the maximum critical current occurs at a non-zero magnetic field, which is completely different to the Fraunhofer-type behavior. Second, there is a finite modulation period on each junction although the periods are different on each junction. These behaviors are similar to other  $45^\circ$  asymmetric junctions, which have been analyzed with a large number of 0 and  $\pi$  junctions across the width of the junction

due to the faceting effect.<sup>11,30</sup> For a dominant  $d_{x^2-y^2}$ -wave symmetry, the  $I_c(B)$  pattern of the junction would show a symmetrical pattern with respect to the field polarity with either a dip or tip on  $I_c$  value at zero field, depending on the details of the facet (Fig. 1). However, the pattern will change dramatically when there is a very small percentage,  $\epsilon$ , of secondary phase. In the case of a real  $s$  wave, i.e.,  $d_{x^2-y^2} + \epsilon s$ , the  $I_c$  value at zero field will increase significantly while the field polarity remains symmetrical.<sup>12</sup> On the other hand, an imaginary  $is$  or  $id_{xy}$  phase will distort the field polarity symmetry [Fig. 1(a) and Ref. 12]. Therefore, an onset of secondary phases can be monitored by the change in the  $I_c(B)$  patterns at different temperatures.

The  $I_c(B)$  patterns of A2 and A4 are not highly symmetrical with respect to any point of the magnetic field and apparently a symmetrical point can be defined at the dip of  $B \sim -10 \mu\text{T}$  on both junctions [Fig. 4(a)]. This offset can also be observed during the measurements on some of the other junctions. This may be a result of a residual field present inside the mu-metal shield of the probe during cool down. The asymmetry of field polarity in A2 and A4 could be due to the self-field effect as their width is slightly larger than  $\lambda_J$ . Figures 4(b) and 4(d) show the  $I_c(B)$  patterns of junctions B1 and C1 at different temperatures. The patterns are symmetrical at high-temperature measurements whereas it became asymmetrical at lower temperatures for B1. However, the symmetry is still maintained at lower temperatures on C1. Although B1 and C1 are both in the short-junction limit, in which the self-field effect can be excluded, some of the facets with local  $J_c$  higher than the average junction  $J_c$  might introduce a self-field effect and induce asymmetry for a symmetrical pattern. Measurements of negative critical current can be used to test the origin of the asymmetry in  $I_c(B)$ . Asymmetrical  $I_c(B)$  on both positive and negative currents due to the self-field effect would be symmetric through the origin, whereas asymmetry due to MOPS would be symmetric through the  $x$  axis.<sup>31</sup> Therefore, we also measured the negative current diffraction pattern of B1 at 4.3 K [Fig. 4(c)]. The symmetry of  $I_c(B)$  through the magnetic-field axis excludes the self-field effect. According to the calculations on Fig. 1(a), the asymmetry is likely to be due to the onset of an imaginary (out-of-phase) subdominant component on the interface of the junction. Note that a secondary out-of-phase  $d_{xy}$  component could also introduce polarity asymmetry with

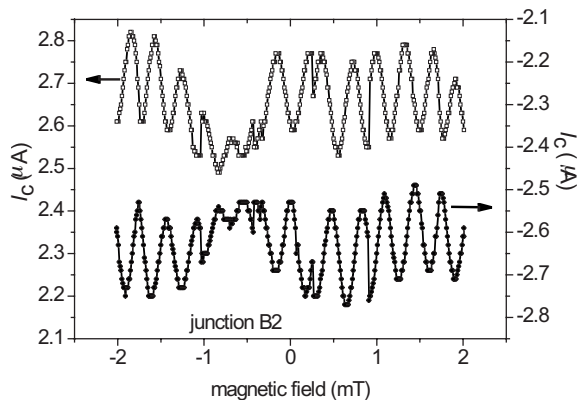


FIG. 5. The positive and negative  $I_c(B)$  of B2 at 4.3 K.

similar order of magnitude.<sup>12</sup> Flux jumps can sometimes be observed at high-temperature measurements, e.g., sample B1 at 35.6 K, which is believed to be due to the entry of vortex close to the junction.<sup>32</sup> The typical value of magnetic field at vortex entry,  $B_c$ , is  $\sim 1$  mT. However, this behavior was not

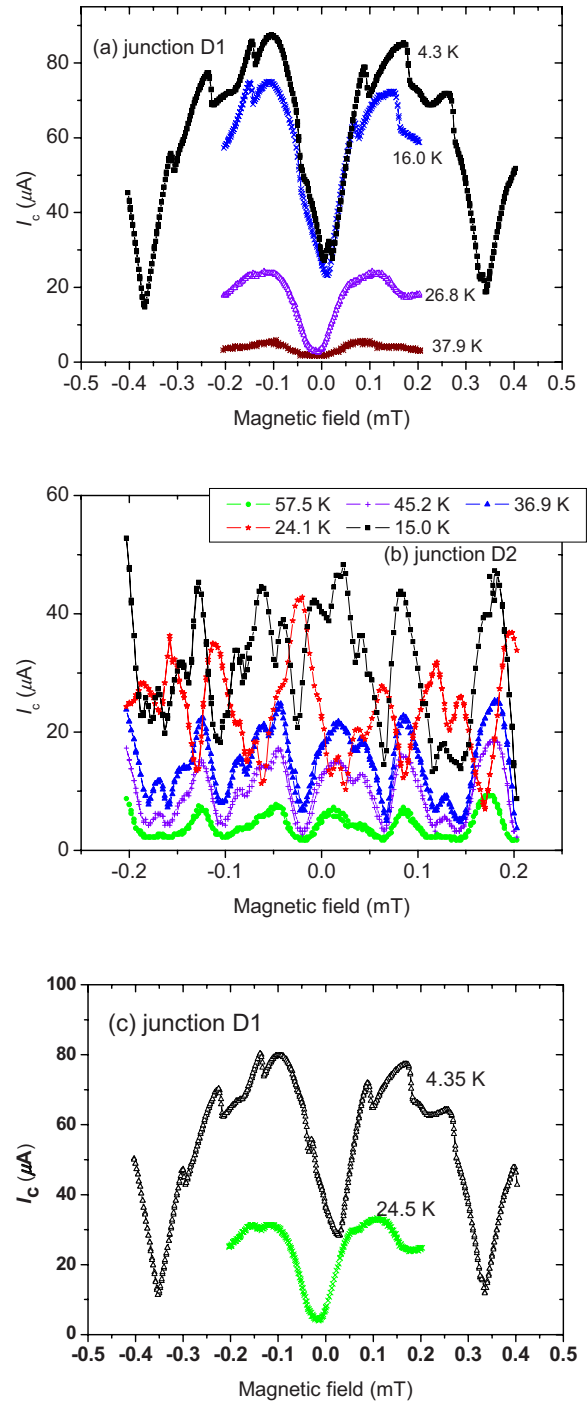


FIG. 6. (Color online)  $I_c(B)$  of D1 (a) and D2 (b) at different temperatures. A symmetrical point can be defined at the dip of  $\sim -15 \mu\text{T}$ . The offset from zero magnetic field may indicate a residual field is present inside the mu-metal shield of the probe during cool down. (c)  $I_c(B)$  of D1 at two different temperatures after the sample has been warmed up to  $\sim 100$  K (above its critical temperature) and cooled down.

observed at temperatures below  $\sim 30$  K perhaps due to the increment of  $B_c$  beyond the magnetic-field range in our experiment as temperature decreases. Therefore, it is believed that the asymmetrical  $I_c(B)$  pattern observed at low temperatures is not due to flux trapping near the junction.

Figure 5 shows the  $I_c(B)$  of junction B2 measured at 4.3 K. B2 has a  $R_n A$  value similar to B1 but the  $I_c$  value is ten times smaller (Table I). Asymmetry in field polarity was also observed in this junction. We have attempted to measure the  $I_c(B)$  at higher temperatures but the  $I_c$  value becomes too small and noisy due to the thermal activated phase slip.<sup>33</sup> It is difficult to obtain the ratio between the  $s$  and  $d$  waves,  $\varepsilon$ , by directly comparing the stimulations to the experimental results. We attempt to use the method proposed by Neils and Van Harlingen<sup>12</sup> to quantify the degree of asymmetry,  $\alpha_e$ , where  $\alpha_e(B) = \{[I_c(+B) - I_c(-B)]/[I_c(+B) + I_c(-B)]\}$ , averaged over values of applied flux from the field range in our experiment. Then the calculated value of  $\alpha_e$  can be compared with the stimulation value of  $\alpha_s$ , in which certain value of  $\varepsilon$  was used.<sup>12</sup> The  $\alpha_e$  values of B1 and B2 at 4.3 K [Figs. 4(c) and 5] were found to be 10% and 14% corresponding to a value of  $\varepsilon \sim 0.2$  and 0.25, respectively.  $I_c(B)$  measurements have also been reported on different HTSC junctions,<sup>11–13,34</sup> but significant asymmetry in field polarity have not been observed. On the other hand, the values of  $\alpha_e$  and  $\varepsilon$  are only 1.5% and  $\sim 0.03\%$ , respectively, for C1 [Fig. 4(d)]. The exact reason for the discrepancy with B1 and B2 is unknown. If the grain boundary junction's transmission coefficient is high, the interface does not allow sufficient Andreev reflection to produce ZEBS.<sup>12,17</sup> We note that C1 has a  $J_c$  value of approximately four times larger than that of B1 and B2. The lower transmission coefficient in B1 and B2 could be the reason of the formation of ZEBSs, which suppress the  $d_{x^2-y^2}$  wave, and hence, secondary type pair symmetry can be created. The seed-layer thickness of B1 and B2 is 100 nm, which is much thicker than 30 nm of C1. The 100 nm thick seed layer may introduce a “step-edge” effect near the grain boundary and alter the crystal growth and grain boundary geometry and hence a lower  $J_c$  value compared with a 30 nm seed layer. This is a topic for further investigation.

When we inspect the  $I_c(B)$  patterns of B1 at temperatures below 30 K, we noticed that another peak is formed on each main envelope of the pattern. This can be explained qualitatively by the presence of facets with lower value of critical-current density, which only contribute superconducting current at lower temperatures [Fig. 1(b)]. Coincidentally, it is found that the polarity symmetry is broken when this peak appears. Therefore, we postulate that the onset of the second-

ary phase is at the interface of those facets with a lower value of current density and larger value of specific resistivity, e.g., junctions B1, B2, D1, and D2. Due to the faceting effect, the  $J_c$  and  $R_n A$  values of each miniature junction are different. The “measured”  $J_c$  and  $R_n A$  values are the “average” values of all the miniature junctions (Table I). As they align in a parallel manner, those miniature junctions with larger  $J_c$  and low  $R_n A$  values would “dominate” the measured values and hence it could be the possible reason that the measured  $J_c$  and  $R_n A$  values do not differ considerably from those reported in previous studies.<sup>15</sup> The effect on the variation in critical-current density among facets [Fig. 1(b)] can also be observed in other junctions. Figure 6 shows the  $I_c(B)$  of junctions D1 and D2. In Fig. 6(a), up to four dips can be observed in the main envelope and there is asymmetry in field polarity at lower temperatures. In Fig. 6(b), it was noticed that there is a change in a dip to a peak and then change to a dip again as temperature decreases. This is consistent to the calculation on Fig. 1(b) when more facets start to contribute  $I_c$  to the junction, e.g., at lower temperatures.

Samples B1 and D1 have been warmed up to  $\sim 100$  K (above its critical temperature) and cooled down. The  $I_c(B)$  patterns were measured at two different temperatures and the results [Fig. 4(e) for B1 and Fig. 6(c) for D1] also show asymmetrical pattern, similar to the previous measurement.

## V. CONCLUSIONS

In summary, we have demonstrated a  $45^\circ$  asymmetrical bi-epitaxial YBa<sub>2</sub>Cu<sub>3</sub>O<sub>x</sub> grain boundary Josephson junction and used it as a test bed to investigate the onset of subdominant order symmetry in HTSC. We observed the breaking of polarity symmetry in the  $I_c(B)$  pattern, which is consistent to the prediction of MOPS due to the onset of an out-of phase subdominant order parameter. This is a consequence of the presence of ZEBS near the interface, which suppresses the dominant  $d_{x^2-y^2}$  wave. In some samples, we estimate an imaginary subdominant symmetry greater than 20% to the  $d$  wave at low temperatures, which has not been observed before on other junctions using this measurement technique. From the experimental results on different junctions, we argue that the formation of the secondary phase largely depends on the properties of the barrier interface. The effect of variation in individual facets' critical-current density has also been studied to explain the transport properties of the junctions. We are investigating the dependence of junction parameters with the YSZ thickness to better understand the cause on the difference between junctions with different YSZ thicknesses.

<sup>1</sup>C. C. Tsuei and J. R. Kirtley, Rev. Mod. Phys. **72**, 969 (2000).

<sup>2</sup>D. J. Van Harlingen, Rev. Mod. Phys. **67**, 515 (1995).

<sup>3</sup>M. Sigrist, Prog. Theor. Phys. **99**, 899 (1998).

<sup>4</sup>T. Lofwander, V. S. Shumeiko, and G. Wendin, Supercond. Sci. Technol. **14**, R53 (2001).

<sup>5</sup>C. R. Hu, Phys. Rev. Lett. **72**, 1526 (1994).

<sup>6</sup>D. J. Van Harlingen, J. E. Hilliard, B. L. T. Plourde, and B. D. Yanoff, Physica C **317-318**, 410 (1999).

<sup>7</sup>M. Covington, M. Aprili, E. Paraoanu, L. H. Greene, F. Xu, J. Zhu, and C. A. Mirkin, Phys. Rev. Lett. **79**, 277 (1997).

<sup>8</sup>A. Sharoni, O. Millo, A. Kohen, Y. Dagan, R. Beck, G. Deutscher, and G. Koren, Phys. Rev. B **65**, 134526 (2002).

- <sup>9</sup>M. R. Beasley, D. Lew, and R. B. Laughlin, *Phys. Rev. B* **49**, 12330 (1994).
- <sup>10</sup>J. R. Kirtley, C. C. Tsuei, A. Ariando, C. J. M. Verwijs, S. Harkema, and H. Hilgenkamp, *Nat. Phys.* **2**, 190 (2006).
- <sup>11</sup>C. A. Copetti, F. Ruders, B. Oelze, Ch. Buchal, B. Kabius, and J. W. Seo, *Physica C* **253**, 63 (1995).
- <sup>12</sup>W. K. Neils and D. J. Van Harlingen, *Phys. Rev. Lett.* **88**, 047001 (2002).
- <sup>13</sup>C. W. Schneider, W. K. Neils, H. Bielefeldt, G. Hammerl, A. Schmedl, H. Raffy, Z. Z. Li, S. Oh, J. N. Eckstein, D. J. Van Harlingen, and J. Mannhart, *Europhys. Lett.* **64**, 489 (2003).
- <sup>14</sup>H. J. H. Smilde, Ariando, D. H. A. Blank, G. J. Gerritsma, H. Hilgenkamp, and H. Rogalla, *Phys. Rev. Lett.* **88**, 057004 (2002).
- <sup>15</sup>H. Hilgenkamp, J. Mannhart, and B. Mayer, *Phys. Rev. B* **53**, 14586 (1996).
- <sup>16</sup>T. Ortlev, Ariando, O. Mielke, C. J. M. Verwijs, K. F. K. Foo, H. Rogalla, F. H. Uhlmann, and H. Hilgenkamp, *Science* **312**, 1495 (2006).
- <sup>17</sup>G. Testa, E. Sarnelli, A. Monaco, E. Esposito, M. Ejrnaes, D.-J. Kang, S. H. Mennema, E. J. Tarte, and M. G. Blamire, *Phys. Rev. B* **71**, 134520 (2005).
- <sup>18</sup>T. Bauch, T. Lindstrom, F. Tafuri, G. Rotoli, P. Delsing, T. Claesson, and F. Lombardi, *Science* **311**, 57 (2006).
- <sup>19</sup>S. Gnanarajan and N. Savvides, *Thin Solid Films* **350**, 124 (1999).
- <sup>20</sup>C. P. Foley, E. E. Mitchell, S. K. H. Lam, B. Sankrithyan, Y. M. Wilson, D. L. Tilbrook, and S. J. Morris, *IEEE Trans. Appl. Supercond.* **9**, 4281 (1999).
- <sup>21</sup>S. Gnanarajan, A. Katsaros, and N. Savvides, *Appl. Phys. Lett.* **70**, 2816 (1997).
- <sup>22</sup>H. Hilgenkamp and J. Mannhart, *Appl. Phys. A: Mater. Sci. Process.* **64**, 553 (1997).
- <sup>23</sup>M. F. Chisholm and S. J. Pennycook, *Nature (London)* **351**, 47 (1991).
- <sup>24</sup>J. A. Alarco and E. Olsson, *Phys. Rev. B* **52**, 13625 (1995).
- <sup>25</sup>P. J. Martin and R. P. Netterfield, *Handbook of Ion Beam Processing Technology* (Noyes, Princeton, NJ, 1989), p. 374.
- <sup>26</sup>W. Prusseit, R. Nemetschek, R. Semerad, K. Numssen, R. Metzger, C. Hoffmann, and A. Lümkmann, *Physica C* **392-396**, 801 (2003).
- <sup>27</sup>A. Barone and G. Paterno, *Physics and Applications of the Josephson Effect* (Wiley, New York, 1982), Chap. 6.
- <sup>28</sup>A. Barone, F. Lombardi, A. Monaco, E. Sarnelli, F. Tafuri, and G. Testa, *Phys. Status Solidi B* **241**, 1192 (2004).
- <sup>29</sup>B. Batlogg, *Physica B (Amsterdam)* **169**, 7 (1991).
- <sup>30</sup>R. G. Mints and V. G. Kogan, *Phys. Rev. B* **55**, R8682 (1997).
- <sup>31</sup>W. K. Neils, Ph.D. thesis, University of Illinois at Urbana-Champaign, 2002.
- <sup>32</sup>E. E. Mitchell, C. P. Foley, K.-H. Muller, and K. E. Leslie, *Physica C* **321**, 219 (1999).
- <sup>33</sup>M. Tinkham, *Introduction to Superconductivity* (McGraw-Hill, New York, 1996), p. 210.
- <sup>34</sup>Y. Ishimaru, J. Wen, N. Koshizuka, and Y. Enomoto, *Phys. Rev. B* **55**, 11851 (1997).